

Electronic supporting information for “Cosolvent effects on the structure and thermoresponse of a polymer brush: PNIPAM in DMSO-water mixtures”

Hayden Robertson^a, Andrew R. J. Nelson^b, Stuart W. Prescott^c, Grant B. Webber^a, and Erica J. Wanless^{a,*}

^a*College of Science, Engineering and Environment, University of Newcastle, Callaghan, Australia*

^b*ANSTO, Locked Bag 2001, Kirrawee DC, NSW 2232, Australia*

^c*School of Chemical Engineering, UNSW Sydney, NSW 2052, Australia*

**email: erica.wanless@newcastle.edu.au*

1 FTIR

Fourier-transformed infrared (FTIR) spectroscopy was performed on a Perkin-Elmer FTIR. Each measurement was performed five times over a range of 400–4000 cm^{-1} with 1 cm^{-1} resolution. FTIR spectroscopy probed various DMSO-water mixtures across the entire composition range. Figure S1.1 presents the full spectrum of each sample.

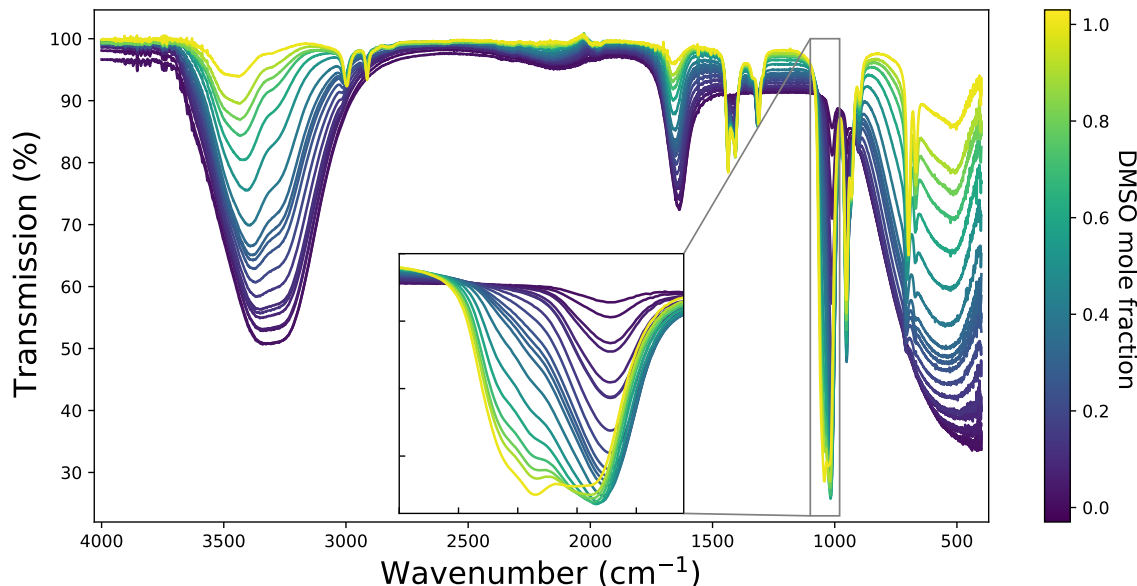


Figure S1.1: FTIR spectra of various DMSO-water mixtures. Magnified inset presents the sulfoxide stretch used in the peak deconvolution; from 900 cm^{-1} to 1130 cm^{-1} .

1.1 Peak deconvolution

Previous studies on these binary mixtures have noted that pure DMSO has a CH_3 rocking mode and $\text{S}=\text{O}$ stretching mode in the region of 980–1100 cm^{-1} .^{1,2} Gaussian peak deconvolution was performed on this region (Figure S1.1 inset). Wallace et al. previously noted that the sulfoxide region for pure DMSO could be deconvoluted into four Gaussian peaks. Here, however, two additional peaks were used in the deconvolution to account for the contributions from H_2O . Figure S1.2 presents both the wavenumber shift and change in amplitude as a function of DMSO content for the CH_3 rocking and $\text{S}=\text{O}$ stretch, however, our discussions will focus on the $\text{S}=\text{O}$ stretching mode.

The $\text{S}=\text{O}$ stretch modes at 1042 cm^{-1} and 1059 cm^{-1} have previously been assigned to contributions from aggregated DMSO and free DMSO monomers, respectively. The presence of DMSO dimers,² as well as longer DMSO oligomers and cyclic structures,¹ have both been previously reported. Briefly, as the intensity of both peaks decreases monotonically from $x_{\text{D}} = 1$ to around the eutectic point, meaning aggregated and self DMSO interactions decrease with increasing water content. In water rich regimes below the eutectic point most DMSO molecules are involved in interactions with water. The intensity and wavenumber of the 1042 cm^{-1} peak exhibits negligible changes up to $x_{\text{D}} = 0.15$, however, a slight subsequent increase in intensity is observed up to around the eutectic point ($x_{\text{D}} \approx 0.33$). Following this, a steep, monotonic increase is observed, pointing towards an increase in DMSO self-association with increasing x_{D} . The intensity of the 1059 cm^{-1} peak is non-monotonic, undergoing an initial decrease, followed by a subsequent increase around the eutectic point. This behaviour arises from the formation of 1DMSO:2 H_2O aggregates, which reach a maximum population at the stoichiometric eutectic point of $x_{\text{D}} = 0.33$. Following this concentration, the intensity must increase as DMSO can

no longer be fully hydrated due to an insufficient number of water molecules. With respect to the shift in wavenumbers, for both S=O stretches, the wavenumber is essentially unchanged at low and intermediate concentrations of water. However, in water-rich regimes, the addition of water seems to interrupt and weaken DMSO-DMSO interactions as a redshift is observed for both peaks. These results align with previous conclusions from Wallace et al.¹

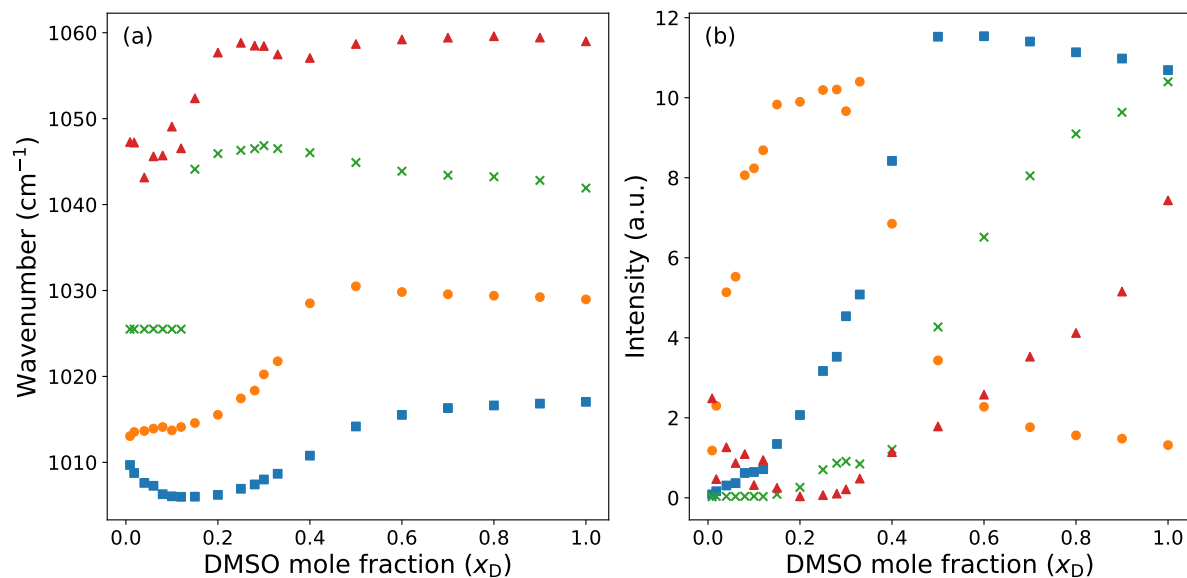


Figure S1.2: Gaussian parameters resulting from the deconvolution of peaks within the region $980\text{-}1100\text{ cm}^{-1}$. (a) Wavenumber shift and (b) change in amplitude as a function of DMSO mole fraction. Modes at both 1017 cm^{-1} (■) and 1029 cm^{-1} (●) relate to the CH_3 rocking of DMSO, whereas peaks at 1042 cm^{-1} (×) and 1059 cm^{-1} (▲) have been assigned to the S=O stretch.^{1,2}

2 Ellipsometry

In binary mixtures up to $x_D = 0.10$, PNIPAM exhibits LCST behaviour. By fitting a logistical function to the swelling ratio data presented in Figure 1 (Equation S2.1), the thermotransition (or LCST) can be extracted as g . The resultant LCST values are presented in Figure S2.1, illustrating a non-linear trend with increasing x_D . Relevant data and Jupyter notebooks containing fitting procedures are readily available on the Zenodo repository.³

$$a + \frac{b - a}{c + d \exp(-e(t - g))^{1/f}} \quad (\text{S2.1})$$

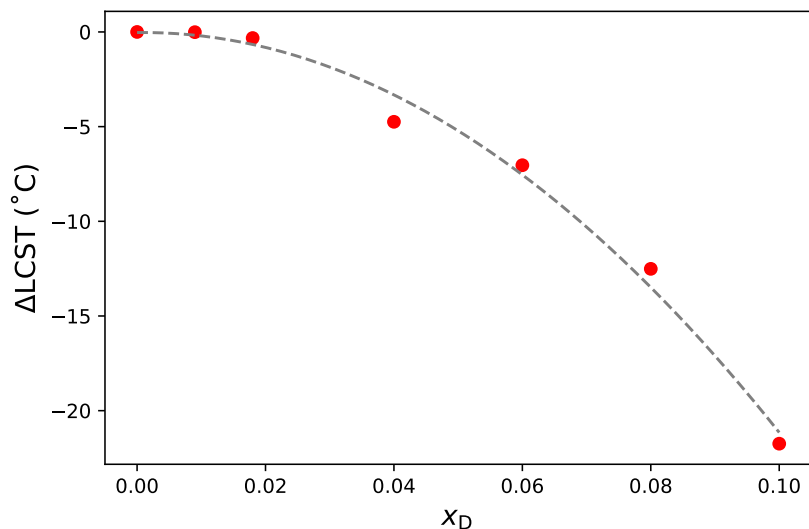


Figure S2.1: Change in LCST (relative to water) of a PNIPAM brush as a function of solvent composition. Dashed line to guide the eye.

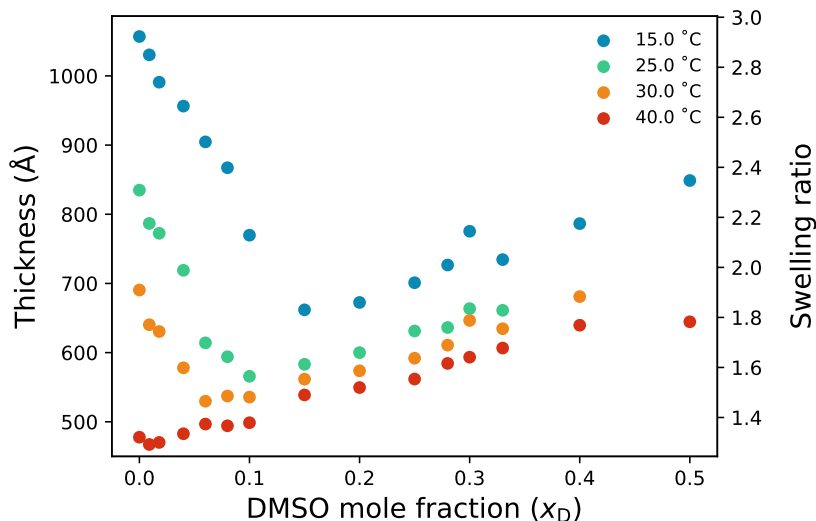


Figure S2.2: Ellipsometry derived brush thickness and swelling ratio of a PNIPAM brush as a function of DMSO mole fraction at select temperatures.

3 Neutron reflectometry

3.1 NR derived brush thickness

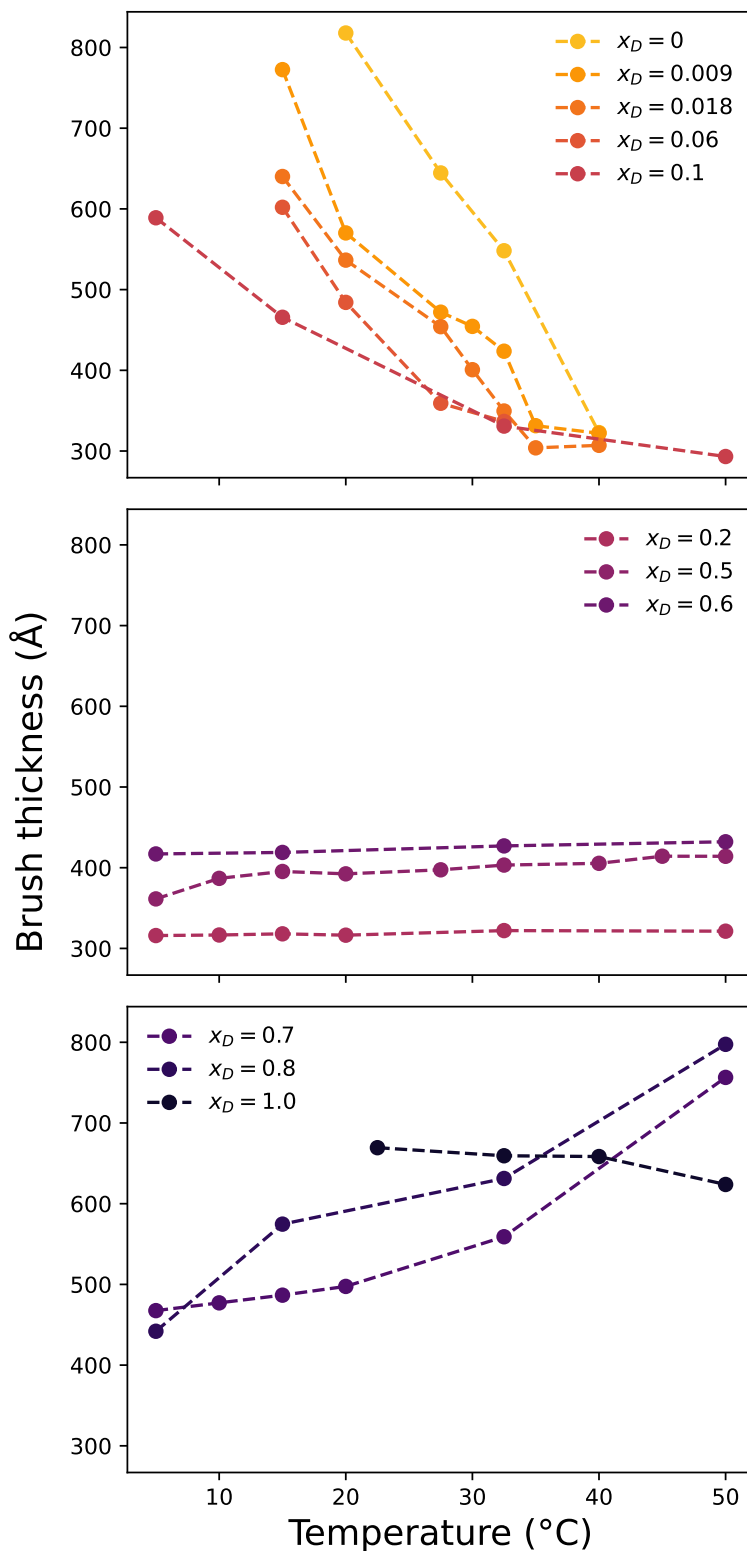


Figure S3.1: NR derived brush thickness as a function of temperature and solvent composition.

3.2 Q-range comparison

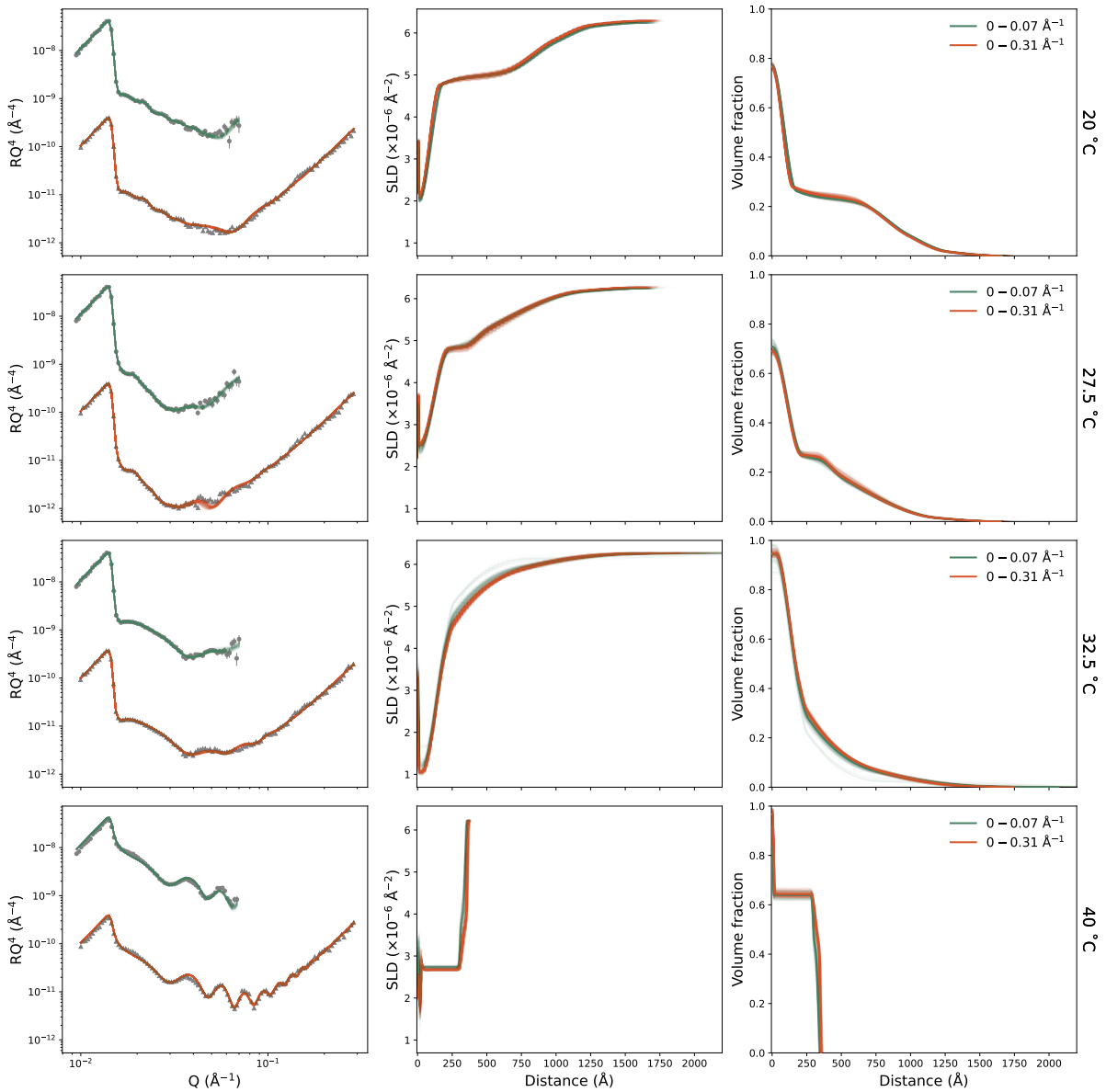


Figure S3.2: Comparison of the distribution of optimised models, SLD and VF profiles against single and double angle reflectivity measurements of a PNIPAM brush in D_2O at 20.0, 27.5, 32.5 and 40.0 °C.

3.3 PT-MCMC Spread of fits

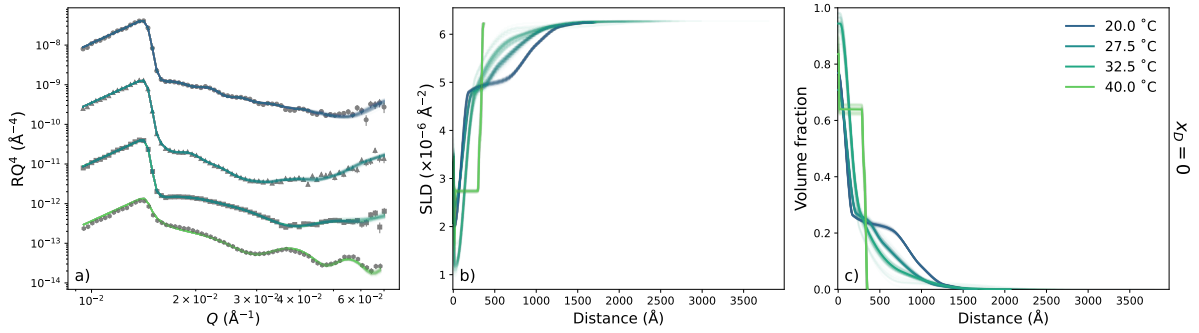


Figure S3.3i: (a) Reflectivity, (b) SLD and (c) polymer VF profiles of the PNIPAM brush with the superimposed distribution of fits from PT-MCMC sampling in $x_D = 0$.

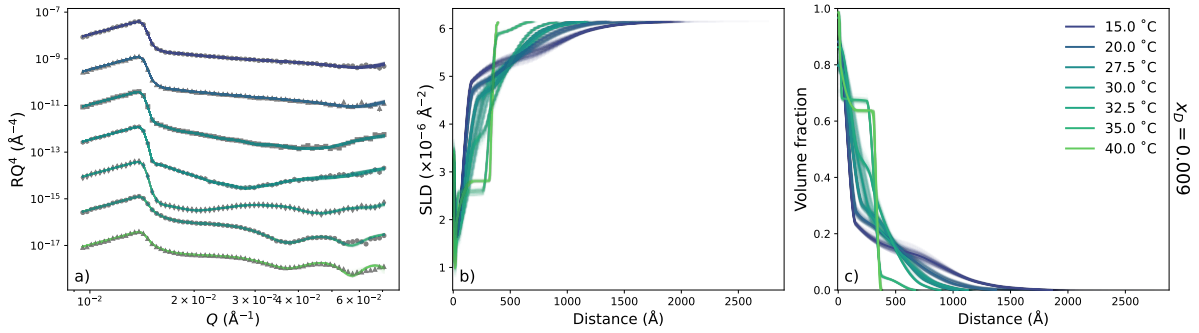


Figure S3.3ii: (a) Reflectivity, (b) SLD and (c) polymer VF profiles of the PNIPAM brush with the superimposed distribution of fits from PT-MCMC sampling in $x_D = 0.009$.

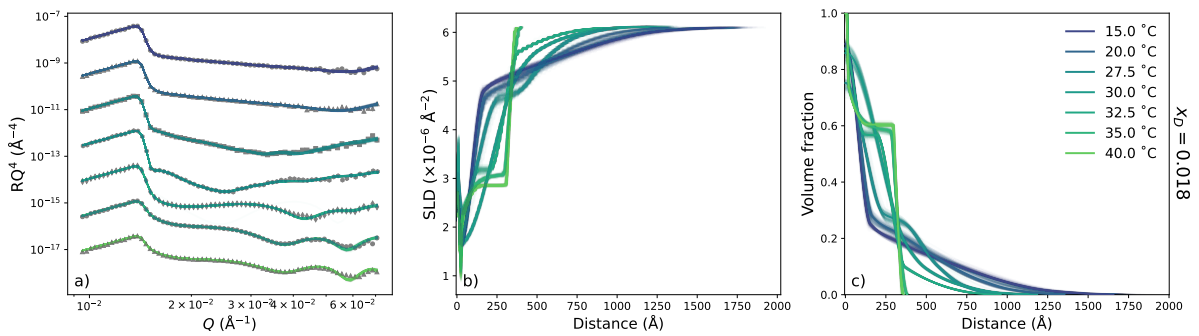


Figure S3.3iii: (a) Reflectivity, (b) SLD and (c) polymer VF profiles of the PNIPAM brush with the superimposed distribution of fits from PT-MCMC sampling in $x_D = 0.018$.

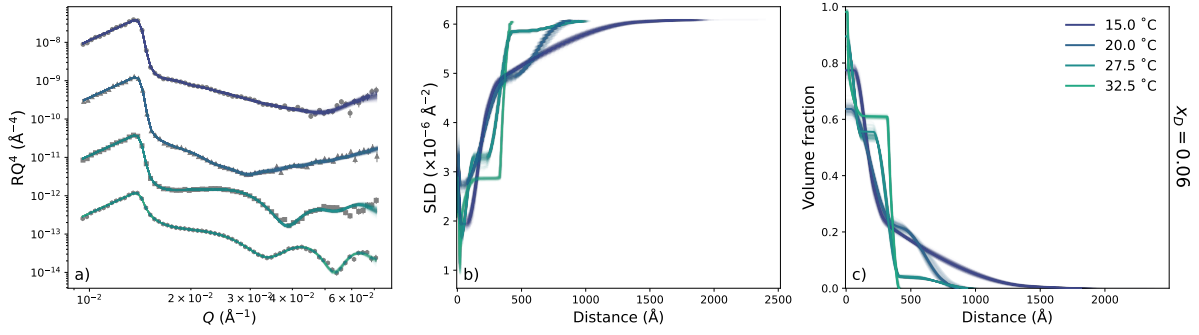


Figure S3.3iv: (a) Reflectivity, (b) SLD and (c) polymer VF profiles of the PNIPAM brush with the superimposed distribution of fits from PT-MCMC sampling in $x_D = 0.06$.

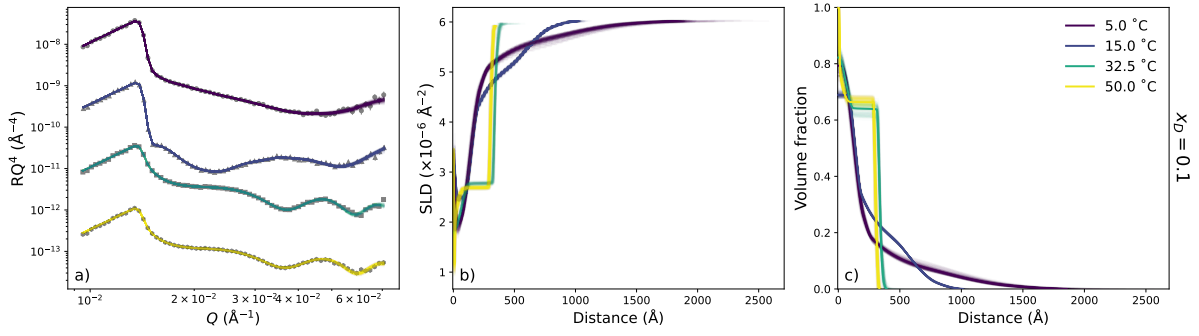


Figure S3.3v: (a) Reflectivity, (b) SLD and (c) polymer VF profiles of the PNIPAM brush with the superimposed distribution of fits from PT-MCMC sampling in $x_D = 0.1$.

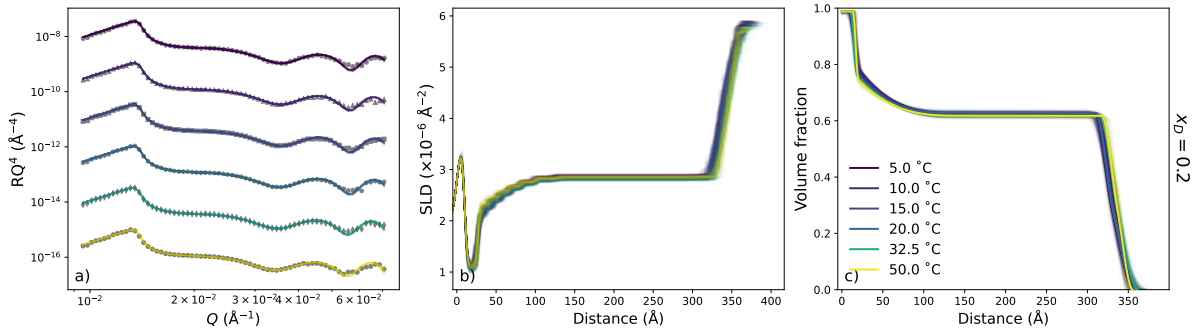


Figure S3.3vi: (a) Reflectivity, (b) SLD and (c) polymer VF profiles of the PNIPAM brush with the superimposed distribution of fits from PT-MCMC sampling in $x_D = 0.2$.

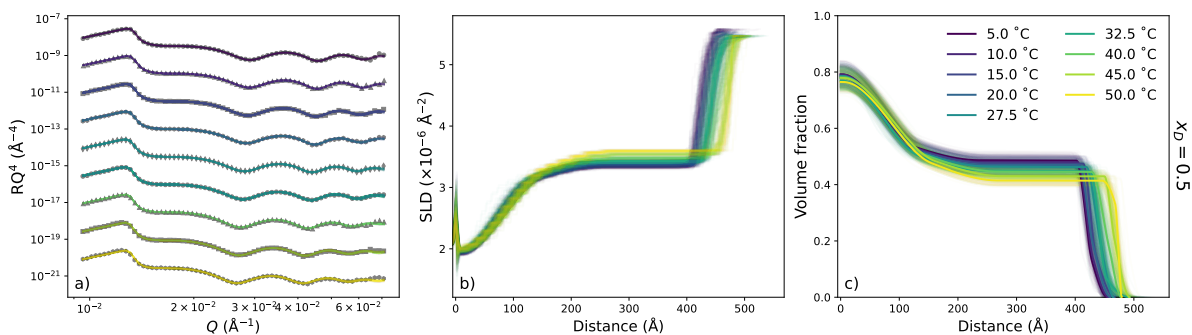


Figure S3.3vii: (a) Reflectivity, (b) SLD and (c) polymer VF profiles of the PNIPAM brush with the superimposed distribution of fits from PT-MCMC sampling in $x_D = 0.5$.

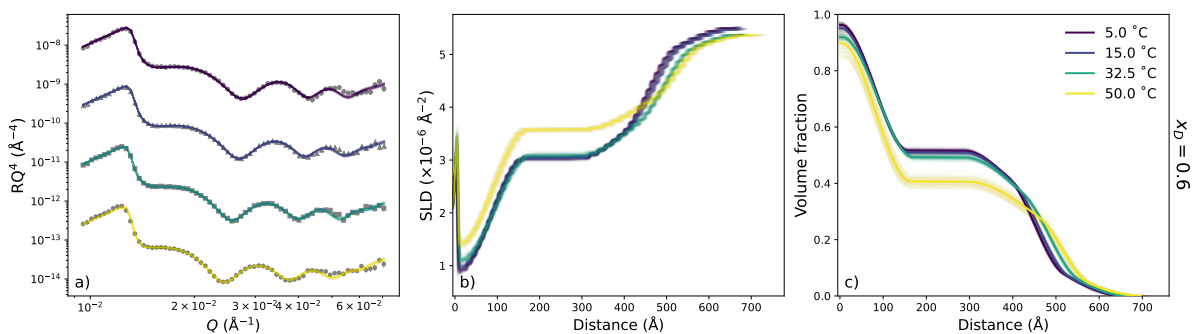


Figure S3.3viii: (a) Reflectivity, (b) SLD and (c) polymer VF profiles of the PNIPAM brush with the superimposed distribution of fits from PT-MCMC sampling in $x_D = 0.6$.

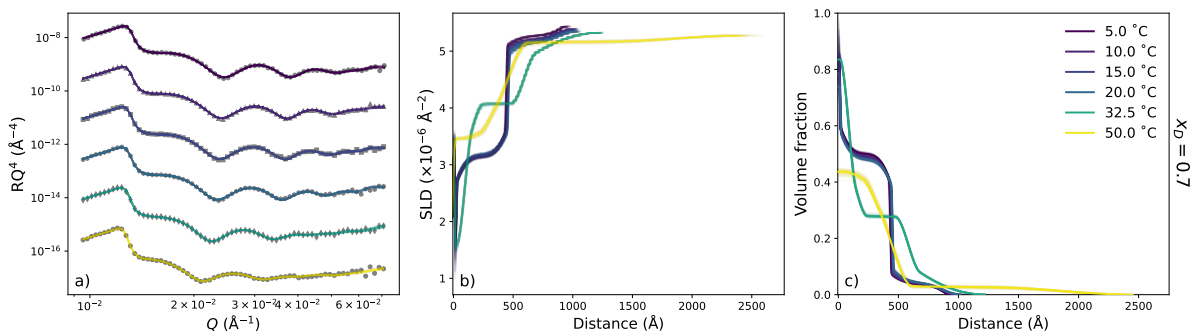


Figure S3.3ix: (a) Reflectivity, (b) SLD and (c) polymer VF profiles of the PNIPAM brush with the superimposed distribution of fits from PT-MCMC sampling in $x_D = 0.7$.

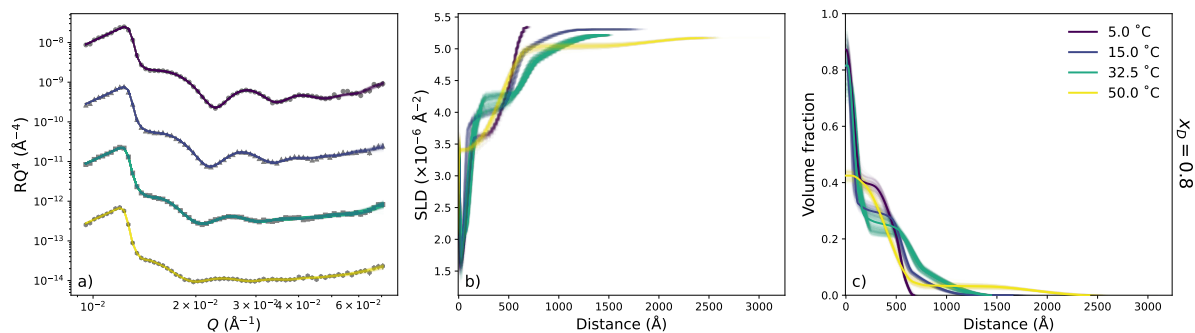


Figure S3.3x: (a) Reflectivity, (b) SLD and (c) polymer VF profiles of the PNIPAM brush with the superimposed distribution of fits from PT-MCMC sampling in $x_D = 0.8$.

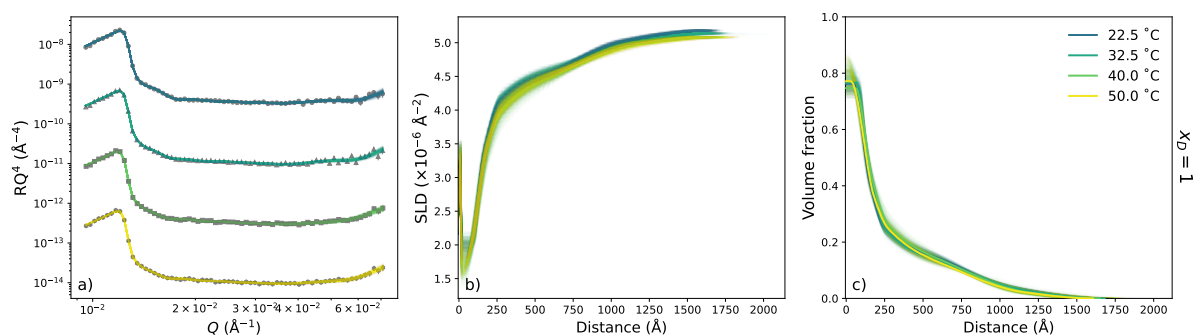


Figure S3.3xi: (a) Reflectivity, (b) SLD and (c) polymer VF profiles of the PNIPAM brush with the superimposed distribution of fits from PT-MCMC sampling in $x_D = 1$.

References

- [1] V. M. Wallace, N. R. Dhumal, F. M. Zehentbauer, H. J. Kim and J. Kiefer, *J. Phys. Chem. B*, 2015, **119**, 14780–14789.
- [2] K.-I. Oh, K. Rajesh, J. F. Stanton and C. R. Baiz, *Angew. Chem. Int. Ed.*, 2017, **129**, 11533–11537.
- [3] H. Robertson, A. R. J. Nelson, S. W. Prescott, G. B. Webber and E. J. Wanless, *Supporting Information for “Cosolvent effects on the structure and thermoresponse of a PNIPAM brush”*, 2022, <https://doi.org/10.5281/zenodo.7359325>, DOI: 10.5281/zenodo.7359325.